Atmósfera 38, 885-910 (2024)
https://doi.org/10.20937/ATM.53380

Chemical and isotopic composition of rainwater in the eastern Yucatan peninsula, Mexico

Daniela ORTEGA-CAMACHO[1], Sofía GONZÁLEZ-RÍOS[2], Fernanda CÓRDOBA-BENAVIDES[2], Luis LADINO[2] and Eduardo CEJUDO[1]*

[1] *Unidad de Ciencias del Agua, Centro de Investigación Científica de Yucatán (CICY-CONAHCyT), Calle 8 núm. 39, Manzana 29, SM 64, 77524 Cancún, Quintana Roo, México.*
[2] *Instituto de Ciencias de la Atmósfera y Cambio Climático, Universidad Nacional Autónoma de México, Circuito Exterior s/n, Ciudad Universitaria, 04510, Ciudad de México, México.*
*Corresponding author; email: eduardo.cejudo@cicy.mx

Received: February 28, 2024; Accepted: May 13, 2024

RESUMEN

La lluvia es el componente de la precipitación que llega a la superficie terrestre. Con el fin de contribuir a los esfuerzos mundiales de monitoreo del agua de lluvia, presentamos información sobre la química del agua y su relación con la composición isotópica y la procedencia de la humedad que puede generar lluvia en el Caribe mexicano. Esta información es útil para estudios atmosféricos y de contaminación, así como para estimaciones de recarga de aguas subterráneas, problemas asociados con el polvo atmosférico y para proporcionar información para la recolección de agua de lluvia. En este artículo describimos la composición química del agua de lluvia (iones mayoritarios), su composición isotópica y las probables fuentes de humedad en la zona costera del Caribe mexicano, considerando las tres estaciones climáticas de esta zona. La química del agua mostró influencia de aerosoles marinos, polvo terrígeno e impactos antrópicos como la agricultura y la quema de biomasa. Identificamos el origen terrestre predominante del calcio, contribuciones antrópicas de sulfatos y nitratos, y potasio proveniente tanto del rocío marino como de emisiones antrópicas. La línea de agua meteórica local es $\delta^2H = 8.2\ \delta^{18}O + 13.8$ ($R^2 = 0.9601$), lo que sugiere un enriquecimiento isotópico debido a pérdidas por evaporación, diferentes fuentes de humedad y efectos climáticos locales. La composición isotópica no fue diferente entre sitios, pero sí por estaciones climáticas, opuesto a la química del agua. Concluimos que la química del agua responde a las condiciones locales de la columna de aire bajo las nubes, mientras que la composición isotópica está influenciada por el origen de la humedad y las condiciones físicas en que el agua se evapora y condensa.

ABSTRACT

Given that rain is the component of precipitation that reaches the surface of the earth, and aiming to contribute to the global efforts of rainwater monitoring, we present information regarding the origin of ions and their relationship with isotopic patterns and the source of moisture for rainwater in the Mexican Caribbean, which not only may be useful for pollution and atmospheric studies, but also for estimating groundwater recharges, understanding dust nuisances, and offering information about water quality for rainwater harvesting. In this paper, we describe the chemical composition of rainwater in terms of major ions, isotopic composition, and the most probable sources of moisture in the Caribbean coastal zone of Mexico, considering the three main climatic seasons in this area. The chemistry of rainwater displayed a noticeable influence from sea-salt spray, land-blown dust, and anthropogenic impacts such as agriculture and biomass burning. We identified the predominant terrestrial origin of calcium, namely anthropogenic contributions of sulfates and nitrates, plus potassium from sea spray and anthropogenic emissions. The local meteoric water line is $\delta^2H = 8.2\ \delta^{18}O + 13.8$ ($R^2 = 0.9601$) suggesting enrichment due to evaporative losses, various moisture sources and local

climatic effects. Although isotope composition was not different by site, it was by season, as opposed to water chemistry. We conclude that the water chemistry responds to the local conditions of the air column below the clouds, while the isotope composition is influenced by the origin of moisture and the physical conditions in which water evaporates and condenses as well.

Keywords: backward air trajectories, biomass burning, isotopes, sea-salt fraction, soil dust.

1. Introduction

Precipitation is the most closely monitored component of the water cycle because of its relevance for agriculture (Ramírez-Villegas and Challinor, 2012), water availability (Guo et al., 2004), and catastrophic hydrometeorological events (Furl et al., 2018). As water evaporates, it separates from the dissolved components and eventually condenses as aerosol particles present in the atmosphere to form liquid droplets, which might precipitate if they reach a size of ca. 1.0 mm (CONAGUA 2003). Precipitation comprises all the water released from the atmosphere, of which rain is the component that reaches the earth's surface; it is measured as the total amount of precipitation received and accounted for in a device, commonly a rain gauge (Davie, 2008). Rainwater is considered a weakly acidic, dilute solution (Hiscock, 2005); it may be a source of calcium, potassium, ammonium, nitrate, chloride, sodium, magnesium, and sulfates from terrestrial or marine origin; such components (in addition to other insoluble particles and gases) precipitate with rain (Hiscock, 2005). Heavy rainfall events have been associated with pollutants and particle washout; for its part, long-duration low-intensity rain might remove fine particles (Oduber et al., 2020). Although aerosol particles are essential for cloud formation and, hence, precipitation development, they can be removed from the atmosphere by wet deposition (below-cloud scavenging). This removal is more efficient for ultrafine and coarse particles and is strongly linked to droplet size and the environment's relative humidity (Ladino et al., 2011).

Some of the most important changes in rainwater chemistry are associated with dust blow, natural biomass burning fires, and anthropogenic pollution. For instance, Oduber et al. (2020) observed that wildfires acidified precipitations, whereas Saharan dust has been associated with high Si, Al, and Ca values. Zhang et al. (2007) attributed the dominance of sulfate, ammonium, and nitrate to contamination from human activities. Due to its acidic nature, rainwater enhances dissolution and influences cave formation (Beddows, 2004); owing to this, it is important to have a thorough knowledge of the water chemistry to understand the initial part of the autogenic recharge process in karstic aquifers, as it is in the case of the Yucatan peninsula. In Mexico, several studies have assessed rainfall chemistry. Báez et al. (1997, 2007) and Pérez-Suárez et al. (2006) obtained the chemical composition (nutrients and major elements) of rain samples in Mexico's central plateau (2600 masl) while exploring the spatial and temporal variation of wet deposits in the metropolitan zone of Mexico City. They found that a large part of the whole of nitrate, ammonium, and sulfate has an urban origin and that rain is important because it dilutes the ionic concentration and also enters pollutants into forest ecosystems. Ramírez et al. (2010) described the chemical composition of rainwater in the largest city in northeastern Mexico (i.e., Monterrey, 500 masl) and found a strong anthropogenic influence from quarry hills and factories, both sources of atmospheric pollution. Bravo et al. (2000) and Cerón et al. (2002) studied the chemical composition of rain on the Caribbean coast in Puerto Morelos (Quintana Roo), 40 km south of Cancún. Not only did the studies above find clear influence from marine aerosols, but also enrichment from crustal and anthropogenic sources, particularly sulfates and nitrates, attributed to atmospheric contamination from Caribbean islands or biomass burning. Despite previous research works in Mexico that have reported on rainfall chemistry, there is still a void regarding rainwater monitoring stations in this area of the world, which would assist in identifying regional and local meteorological phenomena. We aim to contribute with knowledge that helps answer the question regarding the origin of ions and their relationship with isotopic patterns and the origin of rainwater's moisture, which may also be useful in groundwater recharge estimates,

understanding dust nuisances, and providing information on water quality for rainwater harvesting. In this paper, we describe the chemical composition in terms of the major ions and the isotopic composition of rainwater in the Caribbean coastal zone of Mexico. Moreover, the most probable sources were identified by analyzing the chemical composition and source of air parcels considering the three main seasons in this area.

2. Materials and methods

The rainwater sampling took place once a month: for the chemical analyses from November 2018 to December 2019 and for the stable isotope analyses between November 2018 and February 2021. Four locations were chosen for the present study, all in the State of Quintana Roo, no further than 20 km from the coastline of the Mexican Caribbean (Table I). The sampling protocol was performed as described in Cejudo et al. (2022): rainwater from events longer than 20 min (≈ 20 mL) was collected and then transferred into a 4-L plastic container that stored all the water, which represented the accumulated monthly precipitation in composed samples. Finally, 30 mL sub-samples were transferred to high-density polyethylene bottles (HDPE) for later analyses at the University of Waterloo-Environmental Isotope Laboratory (UW-EIL)

Table I. Seasonal precipitation variability in the study area.

	Rainy season	Cold-front season	Dry season
Days	≈150	≈120	≈90
Mean ± SD	181 ± 18	61 ± 30	64 ± 45
Annual rain (%)	67	18	14
Daily rain (mm)	6	2	2

SD: standard deviation.

2.1 Meteorological data

Data on monthly accumulated precipitation were retrieved from the historical database of the Sistema de Información Hidrológica (Hydrological Information System; SIH) of Mexico (SIH, 2023). The data were related to four stations, those closest to the sampling sites (Fig. 1), from November 2018 to March 2021. For characterizing seasonal trends, we defined three seasons based on historical data (1951-2010), as shown in Table I; thereby, the following were proposed: rainy (June to October, ≈ 900 mm precipitation), cold-front (November to February, ≈ 250 mm precipitation), and dry (March to May, <200 mm precipitation).

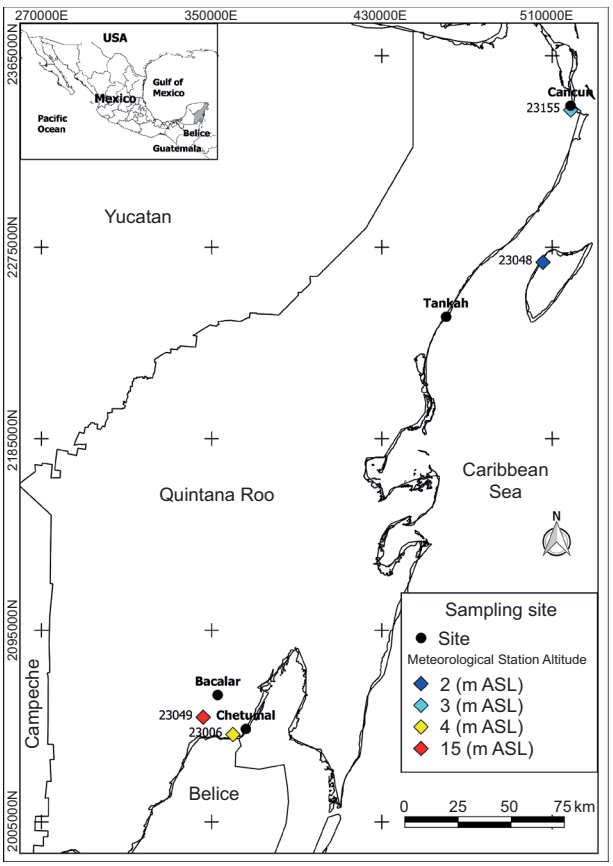

Fig. 1. Sampling sites, altitude (masl), and codes of the nearest meteorological stations.

2.2 Hydrochemistry

The chemical composition of rainwater is represented by the major ions (i.e., sodium, magnesium, potassium, calcium, nitrite, nitrate, sulfate, phosphate, and chloride) measured with an 882 Compact IC Plus ion chromatograph (Metrohm) with a conductivity detector. The samples were stored at room temperature for up to three months, then filtered and analyzed. The anions were quantified under the

following conditions: Metrosep A4 250/4 column with a pre-column Metrosep R2 Guard 3.5, mobile phase 12.6 mM Na_2CO_3/11.9 mM $NaHCO_3$. For their part, conditions for cations were Metrosep C4 250/4 column with a pre-column Metrosep R2 Guard 3.5, mobile phase nitric acid 2.7 mM, and dipicolinic acid. Each sample was analyzed twice with the detection limit of 0.01 mg L^{-1}.

The data normality was evaluated with a Shapiro-Wilk test. Samples that did not have a normal distribution were analyzed with a Kruskal-Wallis test. The rainwater results were analyzed using the volume-weighted mean (VWM) in microequivalents (μeq L^{-1}). The VWM of the various species present in the rainwater samples were calculated using Eq. (1):

$$VWM = \frac{\sum C_i \times P_i}{\sum P_i} \quad (1)$$

where C_i is the concentration of any given ion (μeq L^{-1}) and P_i is the precipitation for the event (mm). For our purposes, each precipitation event comprises the total monthly precipitation, as all analyses were completed in composed water samples accumulated by month, i.e., all the rain events that occur in one calendar month. It is important to note that for the Bacalar sampling site, the chemistry data were only available for five months (i.e., from July to November 2019).

A Pearson correlation was completed for the measured ions. The ion ratio SO_4^{2-}+NO_3^-/ Ca^{2+}+Mg^{2+} was used for assessing the acidity source, where values lower than one (< 1) represent the dominance of alkali ions, and values greater than one (>1) suggest acidic dominance. The NO_3^-+Cl^-/SO_4^{2-} ratio relates to the contribution of either acidic source (nitric or sulfuric); values <1 suggest sulfuric acid-derived acidity, while >1 indicate nitric acid-derived acidity (Salve et al. 2008). The neutralization factor per cation (NF_x) was calculated using Eq. (2) following Oduber et al. (2020):

$$NF_x = \frac{C_x}{\left[C_{SO_4^{2-}} + C_{NO_3^-}\right]} \quad (2)$$

where C_x is the concentration of each cation, and CSO_4^{2-} and CNO_3^- are the sulfate and nitrate concentrations (μeq L^{-1}), respectively. We also calculated the ratios between the concentration of elements in the sample ($Cx/C_{r\,sample}$) with C_x for all elements calculated and C_r as the concentration of the reference element. To distinguish the source or origin of the elements in precipitation, we used two sets of calculations; the first ones are seawater (Eq. [3]) and crust (Eq. [4]) enrichment factors (EF), as follows:

$$EF_{seawater} \frac{\frac{C_x}{C_{r\,sample}}}{\frac{C_x}{C_{r\,seawater}}} \quad (3)$$

$$EF_{crustal} \frac{\frac{C_x}{C_{r\,sample}}}{\frac{C_x}{C_{r\,crust}}} \quad (4)$$

The enrichment factors evaluate the same elements in crust ($C_x/C_{r\,crust}$) and seawater ($C_x/C_{r\,sea\,water}$) relative to the reference concentrations in each of these reservoirs. Conventionally, Na is the reference element for seawater, assuming marine origin (Sp/Na; Keene et al., 1986); whilst Ca is the lithophilic reference element for continental crust (Sp/Ca; Zhang et al., 2007). The concentrations utilized in the EF calculations above are expressed in μeq L^{-1}.

The calculations for the contribution of the second source were performed with the sea salt fraction (%SSF, Eq. [5]) and a non-sea salt fraction (%NSSF, Eq. [6]); the former related to the percentage of seawater from sea spray, and the latter to crustal fractions (i.e., terrestrial dust; Zhang et al., 2007). The calculations were as follows:

$$\%SSF = 100 \times \frac{\left(\frac{C_x}{Na}\right)_{seawater}}{\left(\frac{C_x}{Na}\right)_{rainwater}} \quad (5)$$

$$\%NSSF = 100 \times \frac{\left(\frac{C_x}{Ca}\right)_{crust}}{\left(\frac{C_x}{Ca}\right)_{rainwater}} \quad (6)$$

A non-natural or anthropogenic fraction (Eq. [7]) is commonly assumed as the remnant contribution after computing seawater and crust, expressed as the difference from 100%.

$$\%AF = 100 - (\%SFF + \%NSSF) \quad (7)$$

Lastly, a comparison between some rainwater sampling stations worldwide was run to provide the present results with a context.

2.3 Isotopes

The δ^2H $\delta^{18}O$ isotopes were measured at the University of Waterloo Environmental Isotopes Laboratory using a Los Gatos Research (LGR) liquid water isotope analyzer (LWIA), model T-LWIA-45-EP instrument with published precisions of $\delta^2H = \pm 0.3$ ‰ and $\delta^{18}O = \pm 0.1$‰.

The d-excess parameter was obtained as a function of $\delta^{18}O$ by finding *d* in a line of slope = 8 in the d-space (Gat, 2005; Eq. [8])

$$d - excess = \delta^2 H\ (‰) - 8 \times \delta^{18} O\ (‰) \quad (8)$$

Negative or close to zero values for d-excess indicate a possible loss of light isotopes or fractionation of rainwater by evaporation; in this way, two rain samples with a negative value of d-excess were eliminated so that the final number of samples was 100 for subsequent analyses. We carried out a Kolmogorov-Smirnov test for normality. For normally distributed data, we used a two-way ANOVA and a Kruskal-Wallis for non-normally distributed data.

2.4 Backward air parcel trajectories

We used the Hybrid Single Particle Lagrangian Integrated Trajectory model (HYSPLIT; Stein et al., 2015) to obtain the backward trajectories of the air masses to relate moisture sources with the chemical and isotopic composition of the rainwater samples (Burnett et al., 2004). For the present study, and based on our season's classification, we selected September, January, and May as representative months for each season (i.e., rainy, cold-front, and dry season, respectively) to explain the trajectory models. We used the trajectory ensemble mode with a 144-h time window between the days 10 to 15 of each of the selected months (mid-month) at three altitudes (250, 500, and 1000 m above the ground), assuming that the cloud base level in the Yucatan peninsula is around 1000 m (Nuijens et al., 2014; NOAA, 2024). The endpoint of the trajectories corresponds to each sampling location. The seasonal differences in rainwater chemistry, stable isotopes, as well as air parcels were explored based on the year division shown in Table I.

3. Results and discussion

3.1 Hydrochemistry

From the chemical analysis, we found that nitrites (NO_2^-) and phosphates (PO_4^{3-}) were always below the detection limit (< 0.01 mg L^{-1}) in all four sites and that magnesium (Mg^{2+}) was also below such limit in Cancún. Figure 2 shows the results of ion concentrations by sampling site and climatic season; the complete dataset is presented in Table SI in the supplementary material. The anion deficiency associated with the exclusion of HCO_3^- does not seem very relevant (cations vs. anions correlation coefficient, $R^2 = 0.9508$) and might not have had a significant contribution (Keresztesi et al., 2019).

The calculated VWM values are shown in Table III. According to these concentrations, the anions in Cancún, Tankah, and Chetumal have the following trend: $Cl^- > SO_4^{2-} > NO_3^-$; whereas in Bacalar, chloride, and sulfate switch order ($SO_4^{2-} > Cl^- > NO_3^-$). For cations, Tankah and Chetumal have the trend $Ca^{2+} > Na^+ > Mg^{2+} > K^+$, Cancún $Ca^{2+} > Na^+ > K^+ > Mg^{2+}$, and Bacalar $Ca^{2+} > Mg^{2+} > Na^+ > K^+$. In all cases, Ca^{2+} was the predominant cation. Given that soil dust contains calcite minerals from calcium carbonates present in the soil of the region (Bravo et al., 2000), our results reflect the presence of calcium-rich dust in the Yucatan peninsula's atmosphere (Báez et al., 1997; Galloway and Lickens, 1978). Since the calculation of the ion ratio $SO_4^{2-} + NO_3^-/Ca^{2+} + Mg^{2+}$ was found to be < 1, it points to alkali dominance (from calcium and magnesium). Despite the alkaline dominance, the small acidity present in the rainwater samples showed dominance from nitric acid ($NO_3^- + Cl^-/SO_4^{2-} > 1$); only Bacalar has sulfuric acid-dominant acidity (Table III).

The correlation coefficients shown in Table IV suggest that potassium might originate from both sea spray and anthropogenic emissions such as biomass burning (Oduber et al., 2020; Raga et al., 2021). Even though potassium feldspars are present in the carbonaceous shale of this area (Lefticariu et al., 2006), we consider this to be the lesser contribution as it is mainly buried below the actual surface level. Calcium is considered to come from two sources: seawater (the least) and crustal inputs such as soil

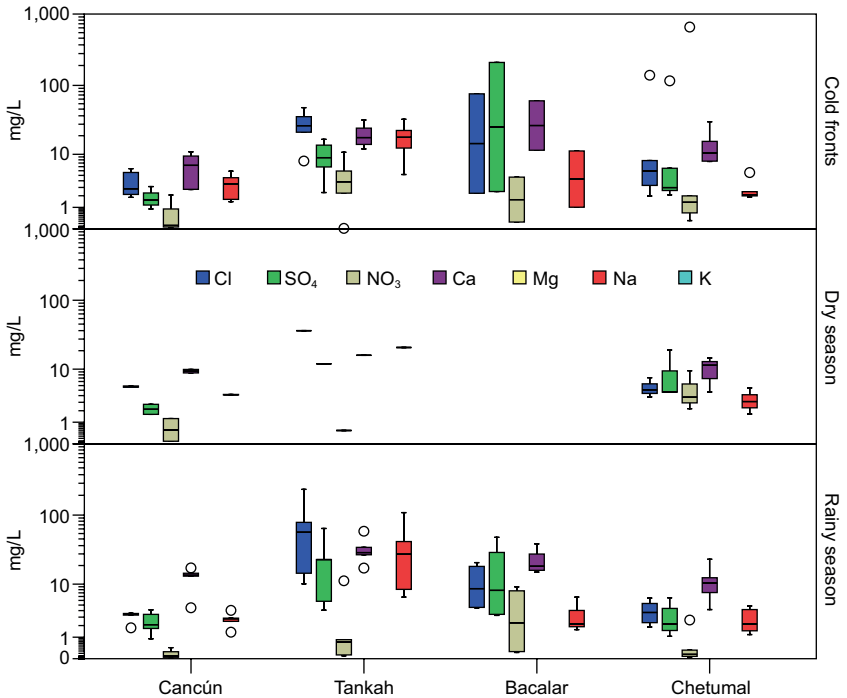

Fig. 2. Box plot of ion concentrations (mg L^{-1}) at each sampling site. Missing values were below the detection limit (< 0.01 mg L^{-1}). Chemical species appear without charge.

The Shapiro-Wilk normality test indicated that none of the ions had a normal distribution ($p < 0.001$); therefore, the Kruskal-Wallis test showed that data from November 2018 to December 2019 was different by site, not by season, as shown in Table II.

Table II. Summary of Kruskal-Wallis test analyses.

	Cl^-	SO_4^{2-}	Ca^{2+}	Mg^{2+}	Na^+	K^+
Site						
χ^2	22.33	19.74	20.52	26.81	23.11	19.44
df	3	3	3	3	3	3
p	**0.0001**	**0.0002**	**0.0001**	**0.00001**	**0.00004**	**0.0002**
Season						
χ^2	0.4	0.52	3.66	0.81	0.47	0.82
df	2	2	2	2	2	2
p	0.82	0.77	0.16	0.67	0.79	0.66

Numbers in bold indicate a statistical difference ($\alpha = 0.05$).

Table III. Volume-weighted mean (meq) measured in rainwater in the coastal zone of Quintana Roo, Mexico.

VWM (meq)	SO_4^{2-}	Cl^-	NO_3^-	HCO_3^-	Ca^{2+}	Mg^{2+}	Na^+	K^+	$SO_4^{2-}+NO_3^-/Ca^{2+}+Mg^{2+}$	$NO_3^-+Cl^-/SO_4^{2-}$
Cancún	0.037	0.098	0.006	0.335	0.362	0.000	0.107	0.010	0.053	2.684
Bacalar	0.409	0.300	0.060	0.800	1.188	0.187	0.135	0.134	0.647	0.795
Tankah	0.224	0.941	0.039	1.086	1.105	0.322	0.818	0.082	0.582	4.246
Chetumal	0.067	0.112	0.020	0.522	0.517	0.060	0.126	0.022	0.165	1.683

Table IV. Correlation coefficients between the major ions measured in rainwater. Numbers in bold indicate a statistical difference (α=0.05)

	SO_4^{2+}	Cl^-	NO_3^-	HCO_3^-	Ca^{2+}	Mg^{2+}	Na^+	K^+
SO_4^{2+}	*1*							
Cl^-	0.380	*1*						
NO_3^-	**0.984**	0.441	*1*					
Ca^{2+}	**0.928**	0.688	**0.954**	**0.898**	*1*			
Mg^{2+}	0.652	**0.938**	0.717	**0.998**	**0.887**	*1*		
Na^+	0.181	**0.978**	0.253	**0.831**	0.527	**0.855**	*1*	
K^+	**0.997**	0.453	**0.989**	0.726	**0.954**	0.711	0.259	*1*

dust (Bravo et al., 2000); however, calcium can also be incorporated into the atmosphere via fertilizers (Zeng et al., 2020), supported by its correlation with NO_3^- (r = 0.954) and sulfates (r = 0.928). The correlation coefficient between SO_4^{2-} and NO_3^- (r = 0.98) suggests a common anthropogenic source due to SO_2 and NO_X in the atmosphere (Zhang et al., 2007; Oduber et al., 2020). There are other ion ratios with good correlation coefficients: Ca^{2+} and SO_4^{2-}; Ca^{2+} and NO_3^-; Mg^{2+} and Cl^-; all of them have a common origin that exists in rainwater as a result of atmospheric chemical reactions of acids such as H_2SO_4, HNO_3, and HCl with alkaline compounds rich in calcium and magnesium, found in the atmosphere from wind-blown dust (Chandra et al., 2005; Salve et al., 2008).

According to the neutralization factor (NF) results (Table V), high NF values for the alkali element Ca^{2+} (from 2.5 to 8.5) are associated with the transport of soil dust with a large quantity of calcite and dolomite due to the calcareous soil of the study area (Peikam and Jalali, 2021).

Table V. Neutralization factor calculated for calcium, magnesium, sodium, and potassium for the four sites

NF	Ca^{2+}	Mg^{2+}	Na^+	K^+
Cancún	8.510	0	2.506	0.235
Bacalar	2.530	0.398	0.287	0.285
Tankah	4.201	1.226	3.108	0.311
Chetumal	5.944	0.685	1.451	0.248

The enrichment factors of the rainwater samples EF_{crust} <1 suggest that the element is mainly from crustal origin; values >1 are associated with other sources, either seawater or anthropogenic origin. The $EF_{seawater}$ for SO_4^{2-}, Ca^{2+}, Mg^{2+}, and K^+ were found to be >1, which indicates enrichment or impacts by sources other than marine; for example, soil or anthropogenic sources (Table VI).

The correlation between Ca and Mg (r = 0.88) indicates crustal origin. In the case of Cl^- its correlations were found to be ≤ 1 in Cancún, Tankah, and Chetumal, indicating an important contribution

Table VI. Summary of the calculated enrichment factors

		SO_4^{2-}	Cl^-	NO_3^-	Ca^{2+}	Mg^{2+}	Na^+
$EF_{seawater}$	Cancún	2.7	0.8	2843.3	77.4	0	4.3
	Bacalar	24.3	1.9	22407.6	200.6	6.1	45.5
	Tankah	2.2	1	2403.2	30.8	1.7	4.6
	Chetumal	4.3	0.8	7736.3	93.3	2.1	7.8
$EF_{crustal}$	Cancún	5.4	87	5.4	0.5	0	71.8
	Bacalar	18.3	81.5	18.3	0.2	0.3	17.6
	Tankah	10.8	274.8	10.8	1.3	0.5	26.8
	Chetumal	6.9	70	6.9	0.4	0.2	47.5

from seawater. This last correlation is consistent with the relationship between Cl^- and Na^+ ions (r = 0.97), whose values are very close to those found in seawater (1.2; Möller, 1990). In sum, our results indicate that chloride, sulfate, sodium, and magnesium are mostly from the sea-salt fraction in the coastal stations (Table VII).

Despite being present in other coastal locations, Mg in Cancún was always below the detection limit. This element has been considered a continental ion tracer linked with economic activities (Bravo et al., 2000). Despite having material extraction sites in the study area, the thickness of the exposed geological formations and the elevated content of calcium carbonate (Smart et al., 2006) might overshadow Mg. Accordingly, calcium is mostly of crustal origin. Potassium, nitrates, and sulfates largely have a non-natural origin (Table VIII); that is, anthropogenic activities in the Yucatan peninsula (Bravo et al., 2000; Raga et al., 2021).

Variable wet and dry deposition has been previously observed in tropical coastal environments (Palani et al., 2012), which can be attributed to meteorological factors such as extreme rain events and air and moisture parcel trajectories (Mullaugh et al., 2013). The coastal sites have chloride and sodium from the sea salt fraction, whereas sulfates, calcium, magnesium, potassium, and nitrates also have a non-sea salt origin. Similar results were reported by Cerón et al. (2002), who found potassium, calcium, and sulfate predominant from the non-sea salt fraction; these authors also stated that nitrate is strongly associated with wind direction and elevated nitrates are related to biomass burning (forest fires); however, supported on the published literature, we consider that sulfate and potassium are the ions most related to biomass burning (Oduber et al., 2020; Raga et al., 2021). Some aerosol particles, such as metals and metal oxides, as well as airborne microorganisms, pose risks to human health (Rodríguez-Gómez et al., 2020) or the environment (Rahim et al., 2019), whereas hurricanes might represent additional entrance of ions, potentially posing dangerous wet deposition into the ecosystem (Qiu and Felix, 2021).

Table IX shows the chemical composition of rainwater in some stations located in tropical and subtropical zones. Notice, on one side, the great contribution of chloride and sodium in Tankah due to the marine influence, and on the other, the unusual nitrate in Chetumal, which may come from fertilizers (Zunckel et al., 2003). Hence, we can conclude that rainwater chemistry experienced a rather local

Table VII. Sea salt (SSF) and non-sea salt fraction (NSSF) contribution.

		SO_4^{2-}	Cl^-	NO_3^-	Ca^{2+}	Mg^{2+}	K^+
%SSF	Cancún	36.53	126.61	38.34	1.29	–	23.22
	Bacalar	4.12	52.12	4.86	0.50	16.37	2.20
	Tankah	45.68	100.76	45.36	3.25	57.56	21.79
	Chetumal	23.39	130.50	14.09	1.07	48.09	12.75
%NSSF	Cancún	63.47	–26.61	61.66	98.71	–	76.78
	Bacalar	95.88	47.88	95.14	99.50	83.63	97.80
	Tankah	54.32	–0.76	54.64	96.75	42.44	78.21
	Chetumal	76.61	–30.50	85.91	98.93	51.91	87.25

Table VIII. Non-natural or anthropogenic fraction

	SO_4^{2-}	Cl^-	NO_3^-	Na^+	Mg^{2+}	K^+
Cancún	44.8	–27.8	87.3	–94.5	–	75.4
Bacalar	90.4	46.7	95.8	–401.6	–272.8	92.1
Tankah	45.0	–1.1	93.7	19.9	–149.8	74.5
Chetumal	62.2	–31.9	94.3	–134.1	–434.9	85.1

Table IX. Comparison of the chemical composition of rainwater in selected locations (chemical species in μM).

	pH	NO_3^-	Cl^-	SO_4^{2-}	NH_4^+	Na^+	Mg^{2+}	K^+	Ca^{2+}
Hamedan, Iran. 34º 40' N, 48º 30' E (Peikam and Jalali, 2021)	6.8	20	370	175	NA	110	205	40	275
BBSR, Bermuda. 32 º35 'N, 8º 25' W	5	2.9	88.2	35.8	8	58.2	3.1	2.6	6.9
Zhejiang, China 28º 35' N, 120º 0' E (Zhang et al., 2007)	4.54	31.2	8.5	47.6	81.1	6.27	1.8	4.7	23.9
Monteverde, Costa Rica. 10º 18' N, 84º 47' W (Vásquez et al., 2012)	N.A.	14	58	13	4.7	66	10	10	50.5
Mexico City, Mexico. 19º 18'N, 99º 10' W (Báez et al., 1997)	N.A.	41.5	N.A.	65.5	N.A.	N.A.	4.8	N.A.	35.2
Puerto Morelos, Mexico. 20º 50' N, 86º 52' W (Bravo et al., 2000)	5.35	11.4	150.7	12.7	6.4	128	14.3	5.8	8.9
Bacalar	5-6	56.1	581.8	494.4	N.A.	192.6	252.6	121.4	680.2
Cancún	5-6	7	98.1	20.7	N.A.	131.4	N.A.	23.7	231.9
Chetumal	5-6	842.8	414.9	137.6	N.A.	119.2	53.3	21.1	307.6
Tankah	5-6	52.4	1401.5	164.7	N.A.	1173.2	232.6	109.5	629.6

Locations in italics show the results obtained in this research.
N.A.: not available; BBSR: Bermuda Biological Station for Research.

influence from sea-salt spray, land-blown dust, and anthropogenic impacts such as agriculture and biomass burning.

3.2 Isotopes

The local meteoric water line (LMWL) for the coast of Quintana Roo is shown in Figure 3. In comparison with the Global Meteoric Water Line (GMWL), its slightly higher slope (13.802) suggests a greater δ^2H enrichment due to evaporative losses (Clark and Fritz, 1997; Sun et al., 2021). Not surprisingly, the LMWL showed an amount effect (Dansgaard, 1964); that is, an inverse correlation with the amount of rainfall (r = –0.48). Note that the altitude effect is not relevant because all sampling stations are at similar altitudes. We also observed that some samples (Bacalar, October 2019 and June 2020; Cancún, October 2020, Chetumal, May 2019 and June 2020; Table SII in the supplementary material) have a depleted isotopic composition, similar to the water precipitated with hurricanes Delta and Gamma, which comes to show that some monthly

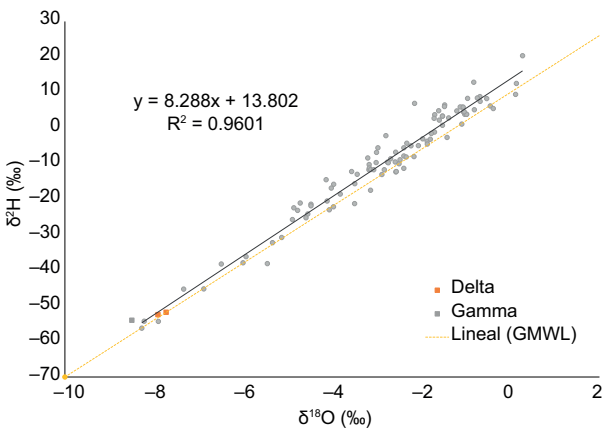

Fig. 3. Local meteoric water line for the Caribbean coast, Quintana Roo, Mexico.

accumulated precipitation samples are isotopically similar to tropical storms.

The high d-intercept value indicated different moisture sources and local climatic patterns (Modon et al., 2022). Some of the most depleted values

correspond to hurricanes Delta and Zeta (–8‰ in $\delta^{18}O$), which were reported as category 2 hurricanes (Sánchez-Murillo et al., 2019). The other main source of moisture comes from North America during the cold-front season (see section 3.3). The local climatic patterns are likely related to convective rains and mixing between two or more air parcels. In coastal locations, convective rains are generally formed from vertically moved ocean-evaporated moisture with high $\delta^{18}O$ (relative to its correspondent $\delta^{2}H$) and have been associated with specific microphysical conditions of rain formation (Aggarwal et al., 2016). The mixing between two or more air parcels does not fit the conventional Rayleigh distillation curve; because of this, the resulting isotopic ratios in tropical and subtropical air parcels are not easily distinguished (Galewsky and Hurley, 2010).

The slope value of the LMWL is slightly greater than those reported for the Cholulteca River basin in Honduras (García-Santos et al., 2022) and the Limbang River basin in Borneo (Modon et al., 2022), which indicates that moisture-generating rain in this area of the world is not formed in equilibrium conditions. The moisture originates in the Caribbean Sea and the Gulf of Mexico with no apparent inputs from the Pacific.

The isotopic composition of each sampling location is shown in Table X. The Kolmogorov-Smirnov test for normality showed that the isotopic composition of the analyzed rainwater samples did not have a normal distribution ($p < 0.001$), whereas d-excess distribution was normal ($K - S = 0.067$; $p = 0.2$). The Kruskal-Wallis test for $\delta^{2}H$ and $\delta^{18}O$ reported that the isotope composition was not different by site ($\delta^{18}O$ ‰ $p = 0.277$ and $\delta^{2}H$ ‰ $p = 0.425$) though it was different by season though ($\delta^{18}O$ ‰ $p = 0.012$ and $\delta^{2}H$ ‰ $p = 0.0003$), a result opposed to that of the water chemistry, which was different by site, but not by season. This difference is because water chemistry and isotope composition respond to different factors and effectors. Water chemistry responds to the local conditions of the air column below the cloud; thus, when precipitation falls, the aerosols and suspended particles reflect the local conditions, with a large influence of marine aerosols and natural and non-natural dust. On the other hand, the isotope composition of moisture has a lesser local influence since its origin (air parcel trajectory) and the physical condition in which water evaporates and condenses are the most relevant factors for variable isotope composition through the seasons.

The d-excess results showed an average of 13.0 ± 3.2 (5.5 to 24.1), similar to other values reported in Central America (García-Santos et al., 2022). The two-way ANOVA for the d-excess showed differences only by season ($F = 12.27$, $p < 0.001$). The post-hoc test Tukey HSD showed that the cold-front season is different ($q = 14.77$, $p < 0.001$). When d-excess values are greater than 10‰, they represent potential re-evaporation of precipitation (Fig. 4); however, such precipitation has also been associated with rain events from cold fronts (García-Santos et al., 2022). It also shows enhanced terrestrial recycled or evaporative moisture sources with similar d-excess. Depleted precipitation due to recycled precipitation has also been reported in Nicaragua (García-Santos et al., 2022).

Table X. Rainwater isotope composition in each sampling location.

Site	Parameter	$\delta^{18}O$ ‰	$\delta^{2}H$ ‰	d-excess
Cancún	Mean	–2.76	–7.99	13.7
	Min–Max	–4.8, –1.02	–25.7, 4.8	9.6, 19.5
Tankah	Mean	–1.69	–1.24	12.4
	Min–Max	–4.4, 0.12	–21.4, 9.4	6.7, 24.1
Bacalar	Mean	–3.48	–16.31	12.3
	Min–Max	–7.3, –0.98	–45.2, 3.8	5.5, 20.2
Chetumal	Mean	–3.11	–10.44	13.6
	Min–Max	–8.2, –0.74	–56.2, 8.4	8.7, 18.3

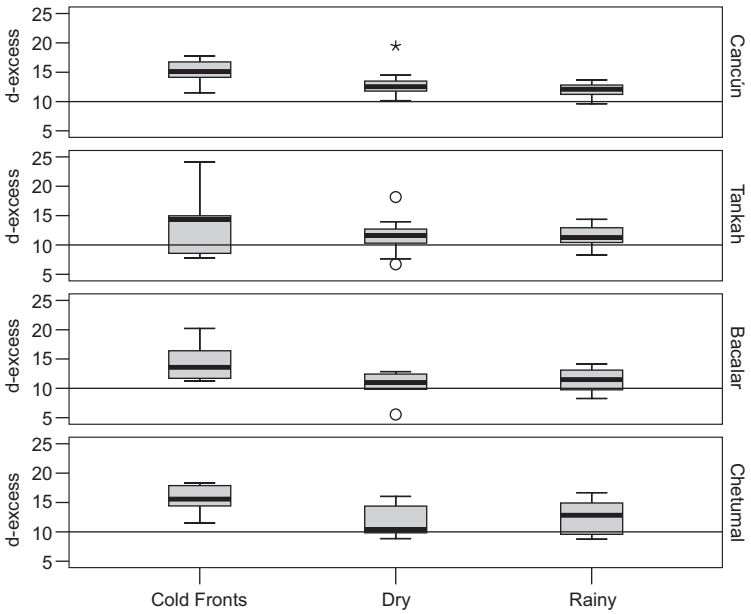

Fig. 4. Deuterium excess values (d-excess) in ‰. The horizontal line in 10 indicates the mean global d-excess value.

Differences in d-excess vary in response to the event type (frontal systems or low-pressure events) or vertical mixing in convective systems rather than seasonal temperature changes (Guan et al., 2013). The elevated d-excess measured in the present study suggests that clouds may be formed in evaporative conditions, and there is mixing of advective condensation in convective rain systems with moisture from the ocean and probably other sources. This phenomenon might be especially relevant in Bacalar, where, based on the lake's water isotope composition, an important amount of moisture may evaporate from Bacalar Lake, condense, and precipitate again (Evans et al., 2018).

3.3 Backward air parcel trajectories

Air parcel trajectories were obtained for the entire sampling period (Fig. S1 in the supplementary material). However, in terms of seasonality, we selected for this study three months (September, January, and May) to represent each of the distinctive seasons in the Yucatan peninsula. Mid-September's rainy season trajectory frequencies (Fig. 5) showed the dominance of east winds from the Caribbean and the mid-Atlantic, passing over Florida and Cuba. These winds probably convey moisture from the mid-Atlantic and the Caribbean into the Yucatan channel, including tropical storms and hurricanes, frequent in this season. The cold-front season trajectory frequencies are exemplified by mid-January in Figure 6, which shows the influence of both north and east winds. The former results from polar air masses moving from the Arctic through North America into the Gulf of Mexico, introducing moisture from the Midwest USA and the Gulf of Mexico into the Yucatan peninsula. This season is characterized by a slightly greater δ^2H (and d-excess) than the other two seasons. Cold-front enriched rains have been previously reported by Sánchez-Murillo et al. (2019) and García-Santos et al. (2022) in the Caribbean. Finally, the dry season trajectory frequencies (mid-May, Fig. 7) depict dominance of east winds from the Caribbean again, but from the east-southeast direction, moving south of Cuba, from the Greater Antilles and the Yucatan basin. These backward air mass movement trajectories suggest that the predominant air mass that reaches the Yucatan peninsula comes from the Caribbean with contributions of terrestrial sources from the islands; consequently, the rain chemistry retains sea salt influence, while a large part of the ions in precipitation moves from the Caribbean most of the year. We acknowledge that the El Niño-Southern Oscillation (ENSO) and the Pacific Decadal Oscillation (PDO) play an important role in rainwater precipitation at a regional scale; yet, a long record

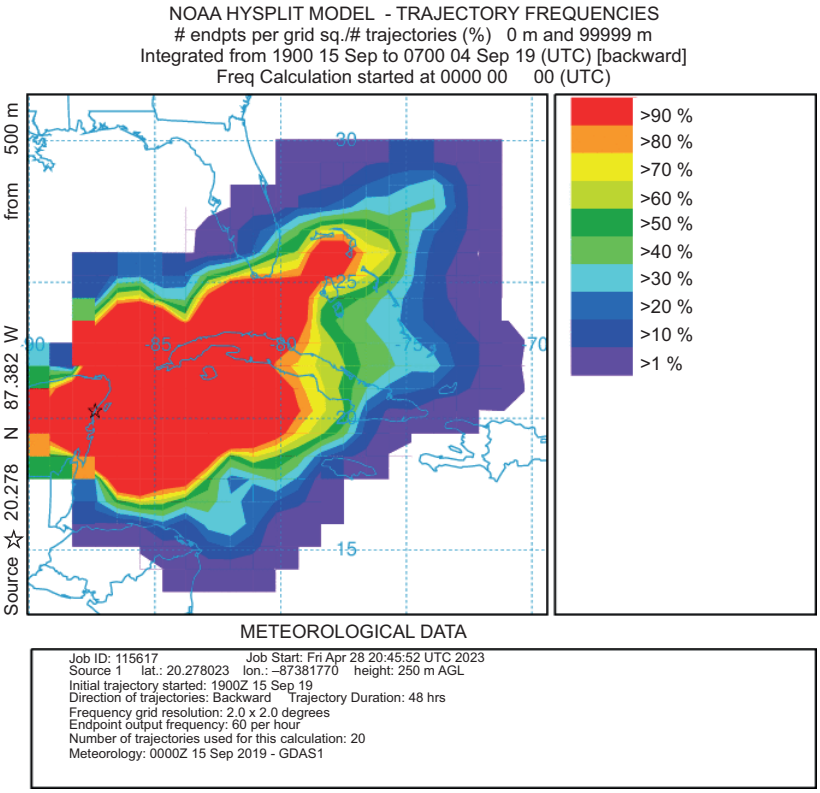

Fig. 5. Backward air parcel trajectories for mid-September 2019.

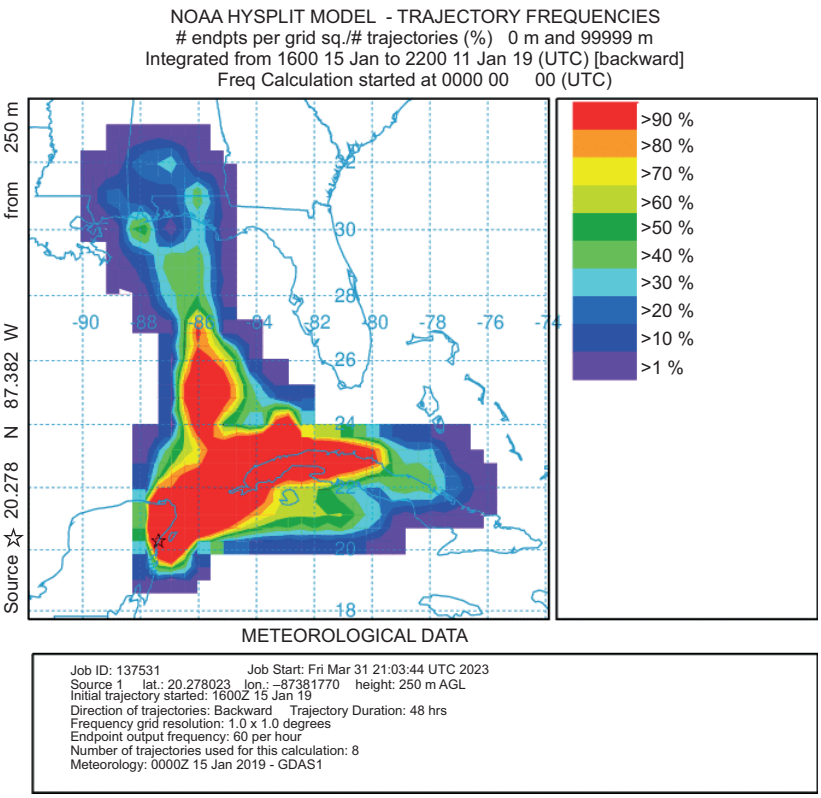

Fig. 6. Backward air parcel trajectories for mid-January 2019.

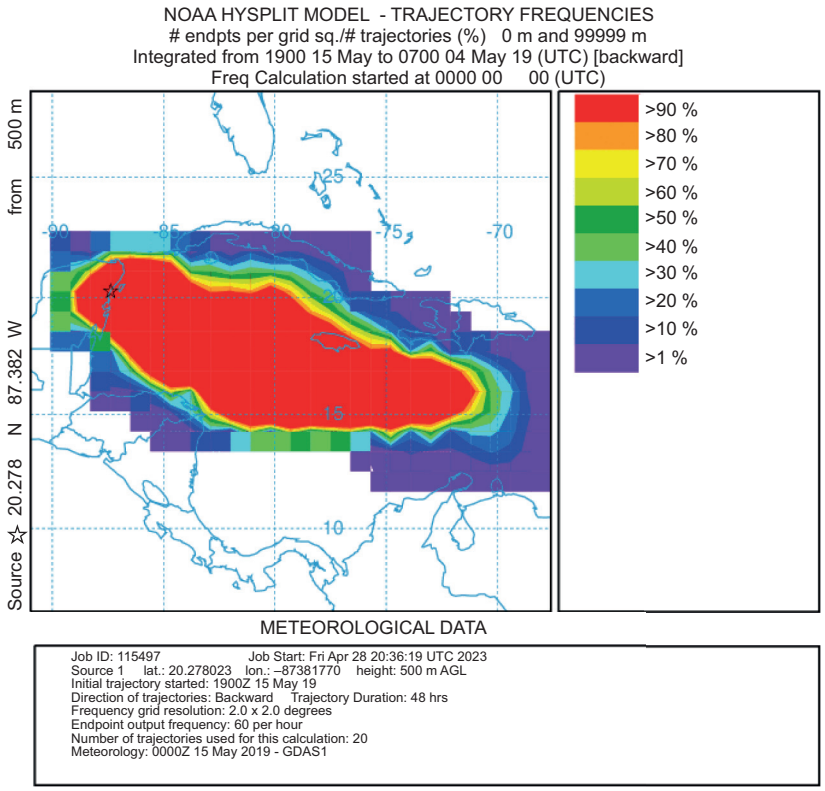

Fig. 7. Backward air parcel trajectories for mid-May 2019.

is necessary to find significant changes in rainfall patterns (Díaz and Giambelluca, 2012), which is out of the scope of this research.

As previously observed in the central Mexican highlands, there is continuous and uniform air parcel movement from the Caribbean Sea (González Ríos, 2022). As there are no topographic barriers, rainfall isotopic pulses are associated with moisture origin (García-Santos et al., 2022) with no isotopic effect due to altitude. This variation in air mass movements is also responsible for variations in rain events, changes in sources of atmospheric moisture, and various evaporation effects, as shown by the isotopic composition.

In addition to the back trajectories of air parcels as tools for exploring moisture sources, atmospheric bulk deposition measurement may be assisted or accompanied by remote sensing (e.g., MODIS) or modeling atmospheric transport; these complementary methods of direct measurement can produce information regarding local or long-distance sources of minerals and contaminants (Das et al., 2013).

4. Conclusions

Chloride, sulfate, sodium, and magnesium are mostly from the sea spray, whereas calcium is mostly crustal. Potassium, nitrates, and sulfates also have a non-natural origin. The rainwater chemistry displayed a local influence from sea-salt spray, land-blown dust, and anthropogenic impacts such as agriculture and biomass burning. The isotope data point to rain not formed in equilibrium conditions, influenced by evaporative losses, different sources of moisture, and local climatic patterns. Our main finding is that water chemistry retains the influence of local conditions such as sea salt, calcium-rich dust, and burnt biomass, whereas the isotope composition showed a less important local influence. The most relevant factors for the observed isotope composition are moisture origin and the physical condition in which water condenses and evaporates. Combined approaches such as the one presented here, with rain chemistry and back trajectories, are of great assistance for more accurate field measurements of nutrient deposition from atmospheric, land, and seaborne sources; also,

they are essential supplies for climate change studies and can be useful to perform groundwater recharge estimations and water quality assessments for rainwater harvesting.

Acknowledgments

Funding was provided by CONACYT Grant CB286049, and Grant Cátedras CONACYT 2944, "Línea de agua meteórica de la peninsula de Yucatán". Irving Escobedo prepared the map presented in Figure 1. We acknowledge Donají Graham, Melina Maravilla, Jacqueline Ann McGrath, and Patricia Fragoso-Servón for collecting and preserving the water samples. Also, Lyssette Muñoz, for the feedback on the early versions of the paper.

References

Aggarwal PK, Romatschke U, Araguas-Araguas L, Belachew D, Longstaffe FJ, Berg P, Schumacher C, Funk A. 2016. Proportions of convective and stratiform precipitation revealed in water isotope ratios. Nature Geoscience 9: 624–629. https://doi.org/10.1038/ngeo2739

Báez AP, Belmont RD, Padilla HG. 1997. Chemical composition of precipitation at two sampling sites in Mexico: A 7-year study. Atmospheric Environment 3: 915-925. https://doi.org/10.1016/S1352-2310(96)00209-9

Báez A, Belmont R, García R, Padilla H, Torres MC. 2007. Chemical composition of rainwater collected at a southwest site of Mexico City, Mexico. Atmospheric Research 86: 61-75. https://doi.org/10.1016/j.atmosres.2007.03.005

Beddows PA. 2004. Yucatán phreas, Mexico. In: Encyclopedia of caves and karst science (Gunn J, Ed.). Taylor & Francis, New York, 1677-1682.

Bravo HA, Saavedra MIR, Sánchez PA, Torres RJ, Granada LMM. 2000. Chemical composition of precipitation in a Mexican Maya region. Atmospheric Environment 34: 1197-1204. https://doi.org/10.1016/S1352-2310(99)00305-2

Burnett AW, Mullins HT, Patterson WP. 2004. Relationship between atmospheric circulation and winter precipitation $\delta^{18}O$ in central New York State. Geophysical Research Letters 31: L22209. https://doi.org/10.1029/2004GL021089

Cejudo E, Acosta-González G, Leal-Bautista RM. 2022. Regional meteoric water line of the Yucatan Peninsula, Mexico. Geoscience Data Journal 9: 124-130. https://doi.org/10.1002/gdj3.123

Cerón RMB, Padilla HG, Belmont RD, Torres MCB, García RM, Báez AP. 2002. Rainwater chemical composition at the end of the mid-summer drought in the Caribbean shore of the Yucatan Peninsula. Atmospheric Environment 36: 2367-2374. https://doi.org/10.1016/S1352-2310(02)00169-3

Chandra Mouli P, Venkata Mohan S, Reddy SJ. 2005. Rainwater chemistry at a regional representative urban site: Influence of terrestrial sources on ionic composition. Atmospheric Environment 39: 999-1008. https://doi.org/10.1016/j.atmosenv.2004.10.036

Clark ID, Fritz P. 1997. Environmental isotopes in hydrogeology. CRC Press, Boca Raton, 342 pp.

CONAGUA. 2023. Glosario técnico. Comisión Nacional del Agua, Mexico. Available at https://smn.conagua.gob.mx/es/smn/glosario (accessed 2023 December 18)

Dansgaard W. 1964. Stable isotopes in precipitation. Tellus A: Dynamic Meteorology and Oceanography 16: 436-468. https://doi.org/10.3402/tellusa.v16i4.8993

Das R, Evan A, Lawrence D. 2013. Contributions of long-distance dust transport to atmospheric P inputs in the Yucatan Peninsula. Global Biogeochemical Cycles 27:167-175. https://doi.org/10.1029/2012GB004420

Davie T. 2008. Fundamentals of hydrology. 2nd ed. Routledge, New York, 221 pp.

Díaz HF, Giambelluca TW. 2012. Changes in atmospheric circulation patterns associated with high and low rainfall regimes in the Hawaiian Islands region on multiple time scales. Global and Planetary Change 98: 97-108. https://doi.org/10.1016/j.gloplacha.2012.08.011

Evans NP, Bauska TK, Gázquez-Sánchez F, Brenner M, Curtis JH, Hodell DA. 2018. Quantification of drought during the collapse of the classic Maya civilization. Science 361: 498-501. https://doi.org/10.1126/science.aas9871

Furl C, Sharif H, Zeitler JW, El Hassan A, Joseph J. 2018. Hydrometeorology of the catastrophic Blanco River flood in South Texas, May 2015. Journal of Hydrology: Regional Studies 15: 90-104. https://doi.org/10.1016/j.ejrh.2017.12.001

Galewsky J, Hurley JV. 2010. An advection-condensation model for subtropical water vapor isotopic ratios. Journal of Geophysical Research: Atmospheres 115: D16116. https://doi.org/10.1029/2009JD013651

Galloway JN, Likens GE. 1978. The collection of precipitation for chemical analysis. Tellus A: Dynamic

Meteorology and Oceanography 30: 71-82. https://doi.org/10.3402/tellusa.v30i1.10318

García-Santos S, Sánchez-Murillo R, Peña-Paz T, Chirinos-Escobar MJ, Hernández-Ortiz JO, Mejía-Escobar EJ, Ortega L. 2022. Water stable isotopes reveal a complex rainfall to groundwater connectivity in central Honduras. Science of the Total Environment 844: 156941. http://doi.org/10.1016/j.scitotenv.2022.156941

Gat JR. 2005. Some classical concepts of isotope hydrology. In: Isotopes in the water cycle: Past, present and future of a developing science (Aggarwal PK, Gat JR, Froehlich KFO, Eds.). Springer, Dordrecht, The Netherlands, 127-137.

González-Ríos S. 2022. Fuentes, orígenes y sistemas de formación de la precipitación en la Ciudad de México, mediante el uso de isótopos estables. B.Sc. thesis. Licenciatura en Ciencias de la Tierra, Facultad de Ciencias, Universidad Nacional Autónoma de México.

Guan H, Zhang X, Skrzypek G, Sun Z, Xu X. 2013. Deuterium excess variations of rainfall events in a coastal area of South Australia and its relationship with synoptic weather systems and atmospheric moisture sources. Journal of Geophysical Research: Atmosphere 118: 1123-1138. https://doi.org/10.1002/jgrd.50137

Guo J, Liang X, Leung LR. 2004. Impacts of different precipitation data sources on water budgets. Journal of Hydrology 298: 311-334. https://doi.org/10.1016/j.jhydrol.2003.08.020

Hiscock KM. 2005. Hydrogeology principles and practice. Oxford UK: Blackwell Publishing.

Keene WC, Pszenny AAP, Galloway JN, Hawley ME. 1986. Sea-salt corrections and interpretation of constituent ratios in marine precipitation. Journal of Geophysical Research: Atmospheres 91: 6647-6658. https://doi.org/10.1029/JD091iD06p06647

Keresztesi Á, Birsan MV, Nita IA, Bodor Z, Szép R. 2019. Assessing the neutralisation, wet deposition and source contributions of the precipitation chemistry over Europe during 2000-2017. Environmental Sciences Europe 31: 50. https://doi.org/10.1186/s12302-019-0234-9

Ladino LA, Stetzer O, Hattendorf B, Günther D, Croft B and Lohmann U. 2011. Experimental study of collection efficiencies of submicron aerosols with cloud droplets. Journal of the Atmospheric Sciences 68: 1853-1864. https://doi.org/10.1175/JAS-D-11-012.1

Lefticariu M, Perry EC, Ward WC, Lefticariu L. 2006. Post-Chicxulub depositional and diagenetic history of the northwestern Yucatan Peninsula, Mexico. Sedimentary Geology 183: 51-69. https://doi.org/10.1016/j.sedgeo.2005.09.008

Möller D. 1990. The Na/Cl ratio in rainwater and the seasalt chloride cycle. Tellus B: Chemical and Physical Meteorology 42: 254-262. https://doi.org/10.3402/tellusb.v42i3.15216

Modon Valappil NK, Mohan Viswanathan P, Hamza V, Sabarathinam C. 2022. Isoscapes to address the regional precipitation trends in the equatorial region of Southeast Asia. Physics and Chemistry of the Earth, Parts A/B/C 127: 103159. https://doi.org/10.1016/j.pce.2022.103159

Mullaugh KM, Willey JD, Kieber RJ, Mead RN, Avery Jr GB. 2013. Dynamics of the chemical composition of rainwater throughout Hurricane Irene. Atmospheric Chemistry and Physics 13: 2321-2330. https://doi.org/10.5194/acp-13-2321-2013

NOAA. 2024. Low clouds. National Weather Service, National Oceanic and Atmospheric Administration, USA. Available at https://www.weather.gov/key/low_clouds (accessed 2024 January 19).

Nuijens L, Serikov I, Hirsch L, Lonitz K, Stevens B. 2014. The distribution and variability of low-level cloud in the North Atlantic trades. Quarterly Journal of the Royal Meteorological Society 140: 2364-2374. https://doi.org/10.1002/qj.2307

Oduber F, Calvo AI, Castro A, Blanco-Alegre C, Alves C, Barata J, Nunes T, Lucarelli F, Nava S, Calzolai G, Cerqueira M, Martín-Villacorta J, Esteves V, Fraile R. 2020. Chemical composition of rainwater under two events of aerosol transport: A Saharan dust outbreak and wildfires. Science of the Total Environment 734: 139202. https://doi.org/10.1016/j.scitotenv.2020.139202

Palani S, Balasubramanian R, Tkalich P. 2012. A 3-D model on the possible role of atmospheric deposition in tropical coastal eutrophication. Contribution to Marine Sciences 2012: 11-21.

Peikam EN, Jalali M. 2021. Chemical composition of rainwater at an urban and two rural stations in the west of Iran, Hamedan. Environmental Earth Science 80: 605. https://doi.org/10.1007/s12665-021-09865-3

Pérez-Suárez M, Cetina-Alcalá VM, Aldrete A, Fenn ME, Landois-Palencia LL. 2006. Química de la precipitación pluvial en dos bosques de la cuenca de la

Ciudad de México. Agrociencia 40: 239-248.

Qiu Y, Felix JD. 2021. Hurricane/tropical storm rainwater chemistry in the US (from 2008 to 2019). Science of The Total Environment. 798: 149009. https://doi.org/10.1016/j.scitotenv.2021.149009

Raga GB, Ladino LA, Baumgardner D, Ramírez-Romero C, Córdoba F, Álvarez-Ospina H, Rosas D, Amador T, Miranda J, Rosas I, Jaramillo A, Yakobi-Hancock J, Kim JS, Martínez L, Salinas E, Figueroa B. 2021. ADABBOY: African dust and biomass burning over Yucatan. Bulletin of the American Meteorological Society 102: E1543-E1556. https://doi.org/10.1175/BAMS-D-20-0172.1

Rahim MF, Pal D, Ariya PA. 2019. Physicochemical studies of aerosols at Montreal Trudeau Airport: The importance of airborne nanoparticles containing metal contaminants. Environmental Pollution 246: 734-44. https://doi.org/10.1016/j.envpol.2018.12.050

Ramírez Lara E, Miranda Guardiola R, Gracia Vásquez Y, Balderas Rentería I, Bravo Álvarez H, Sosa Echeverría R, Sánchez Álvarez P, Alarcón Jiménez A, Torres MC, Kahl J. 2010. Chemical composition of rainwater in northeastern Mexico. Atmósfera 23: 213-224.

Ramírez-Villegas J, Challinor A. 2012. Assessing relevant climate data for agricultural applications. Agricultural and Forest Meteorology 161: 26-45. https://doi.org/10.1016/j.agrformet.2012.03.015

Rodríguez-Gómez C, Ramírez-Romero C, Córdoba F, Raga GB, Salinas E, Martínez L, Rosas I, Quintana ET, Maldonado LA, Rosas D, Amador T, Álvarez H, Ladino LA. 2020. Characterization of culturable airborne microorganisms in the Yucatan Peninsula. Atmospheric Environment. 223: 117183. https://doi.org/10.1016/j.atmosenv.2019.117183

Salve PR, Maurya A, Wate SR, Devotta S. 2008. Chemical composition of major ions in rainwater. Bulletin of Environmental Contamination and Toxicology 80: 242–246. https://doi.org/10.1007/s00128-007-9353-x

Sánchez-Murillo R, Durán-Quesada AM, Esquivel-Hernández G, Rojas-Cantillano D, Birkel C, Welsh K, Sánchez-Llull M, Alonso-Hernández CM, Tetzlaff D, Soulsby C, Boll J, Kurita N, Cobb KM. 2019. Deciphering key processes controlling rainfall isotopic variability during extreme tropical cyclones. Nature Communications 10: 4321. https://doi.org/10.1038/s41467-019-12062-3

SIH. 2023. Sistema de Información Hidrológica, Mexico. Available at https://sih.conagua.gob.mx (accessed 24 September 2023).

Smart PL, Beddows PA, Coke J, Doerr S, Smith S, Whitaker FF. 2006. Cave development on the Caribbean coast of the Yucatan Peninsula, Quintana Roo, Mexico. In: Perspectives on karst geomorphology, hydrology, and geochemistry — A tribute volume to Derek C. Ford and William B. White (Harmon RS, Wicks CM, Eds.). Geological Society of America, Colorado, 105-128. https://doi.org/10.1130/2006.2404(10)

Stein AF, Draxler RR Rolph GD, Stunder BJB, Cohen MD, Ngan F. 2015. NOAA's HYSPLIT atmospheric transport and dispersion modeling system. Bulletin of the American Meteorological Society 96: 2059-2077. https://doi.org/10.1175/BAMS-D-14-00110.1

Sun Z, Hu C, Wu D, Chen G, Lu X, Liu X. 2021. Estimation of evaporation losses based on stable isotopes of stream water in a mountain watershed. Acta Geochimica 40: 176-183. https://doi.org/10.1007/s11631-021-00452-8

Vásquez Morera T, Alfaro Solís R, Sibaja Brenes JP, Esquivel Hernández G, Valdés González J. 2012. Composición química del agua de lluvia y de niebla recolectada en la reserva biológica Monteverde. Uniciencia 26: 51-64.

Zeng J, Han G, Wu Q, Tang Y. 2020. Effects of agricultural alkaline substances on reducing the rainwater acidification: Insight from chemical compositions and calcium isotopes in a karst forests area. Agriculture, Ecosystems & Environment 290: 106782. https://doi.org/10.1016/j.agee.2019.106782

Zhang M, Wang S, Wu F, Yuan X, Zhang Y. 2007. Chemical compositions of wet precipitation and anthropogenic influences at a developing urban site in southeastern China. Atmospheric Research 84: 311-322. https://doi.org/10.1016/j.atmosres.2006.09.003

Zunckel M, Sáizar C, Zarauz J. 2003. Rainwater composition in northeast Uruguay. Atmospheric Environment 37: 1601-1611. https://doi.org/10.1016/S1352-2310(03)00007-4

Table SI. Chemistry dataset

Site	Date	Latitude N	Longitude W	Chloride (mg L^{-1})	Sulfate (mg L^{-1})	Nitrate (mg L^{-1})	Nitrite (mg L^{-1})	Phosphate (mg L^{-1})	Calcium (mg L^{-1})	Magnesium (mg L^{-1})	Sodium (mg L^{-1})	Potassium (mg L^{-1})	PP (mm $month^{-1}$)
Cancún	Nov-18	21.174705	–86.821001	2.78	1.74	0.90	bdl	bdl	5.41	bdl	5.40	1.10	49.2
Cancún	Dec-18	21.174705	–86.821001	5.93	2.90	1.97	bdl	bdl	10.90	bdl	4.18	bdl	58.01
Cancún	Jan-19	21.174705	–86.821001	5.13	2.18	0.10	bdl	bdl	8.27	bdl	3.27	0.42	100.22
Cancún	Feb-19	21.174705	–86.821001	2.03	0.90	0.06	bdl	bdl	2.57	bdl	1.59	bdl	136.8
Cancún	Apr-19	21.174705	–86.821001	5.19	2.56	0.09	bdl	bdl	8.76	bdl	3.81	1.08	47.5
Cancún	May-19	21.174705	–86.821001	5.40	1.58	1.25	bdl	bdl	9.93	bdl	3.89	1.35	30.7
Cancún	Jun-19	21.174705	–86.821001	3.32	3.81	0.10	bdl	bdl	13.20	bdl	3.73	1.80	27
Cancún	Jul-19	21.174705	–86.821001	3.06	3.15	0.02	bdl	bdl	13.64	bdl	2.68	0.88	8.7
Cancún	Aug-19	21.174705	–86.821001	1.70	0.89	<LDM	bdl	bdl	17.48	bdl	1.35	bdl	11
Cancún	Sep-19	21.174705	–86.821001	3.17	1.98	0.08	bdl	bdl	14.60	bdl	2.32	0.56	61.4
Cancún	Oct-19	21.174705	–86.821001	3.27	1.64	0.42	bdl	bdl	4.14	bdl	2.61	bdl	239.51
Cancún	Nov-19	21.174705	–86.821001	1.76	1.16	0.05	bdl	bdl	2.55	bdl	1.40	0.63	173.41
Cancún	Dec-19	21.174705	–86.821001	2.49	1.33	0.14	bdl	bdl	9.39	bdl	bdl	0.51	143.61
Bacalar	Jan-19	18.666993	–88.395663	76.10	210.00	4.28	bdl	bdl	60.61	17.10	11.26	5.71	22.1
Bacalar	Jul-19	18.666993	–88.395663	16.21	17.80	6.81	bdl	bdl	19.92	bdl	bdl	bdl	38.3
Bacalar	Aug-19	18.666993	–88.395663	20.90	48.50	9.03	bdl	bdl	39.12	5.82	6.26	11.31	173
Bacalar	Sep-19	18.666993	–88.395663	4.27	3.02	0.22	bdl	bdl	15.18	1.05	1.55	2.83	86
Bacalar	Oct-19	18.666993	–88.395663	4.11	3.30	0.29	bdl	bdl	17.20	bdl	2.05	2.48	139.7
Bacalar	Nov-19	18.666993	–88.395663	2.15	2.33	0.25	bdl	bdl	11.54	0.59	1.01	1.38	70.3

bdl: bellow detection limit.

Table SI. Chemistry dataset

Site	Date	Latitude N	Longitude W	Chloride (mg L^{-1})	Sulfate (mg L^{-1})	Nitrate (mg L^{-1})	Nitrite (mg L^{-1})	Phosphate (mg L^{-1})	Calcium (mg L^{-1})	Magnesium (mg L^{-1})	Sodium (mg L^{-1})	Potassium (mg L^{-1})	PP (mm $month^{-1}$)
Tankah	Nov-18	20.278023	–87.381770	48.40	11.66	3.43	bdl	bdl	32.11	5.39	32.97	3.84	76.7
Tankah	Dec-18	20.278023	–87.381770	21.40	6.33	2.17	bdl	bdl	12.10	2.87	15.32	1.67	127.9
Tankah	Jan-19	20.278023	–87.381770	32.90	16.81	5.44	bdl	bdl	14.13	4.41	22.72	7.33	159.4
Tankah	Feb-19	20.278023	–87.381770	36.00	13.76	3.68	bdl	bdl	19.08	4.02	21.18	5.39	52.4
Tankah	Apr-19	20.278023	–87.381770	37.10	12.09	0.53	bdl	bdl	16.17	4.34	21.09	6.31	99
Tankah	Jun-19	20.278023	–87.381770	230.00	64.80	11.23	bdl	bdl	59.18	24.90	108.50	10.74	54.7
Tankah	Jul-19	20.278023	–87.381770	57.30	23.24	0.84	bdl	bdl	29.26	6.61	27.78	5.75	22.1
Tankah	Aug-19	20.278023	–87.381770	78.90	23.16	0.71	bdl	bdl	34.88	8.70	42.24	4.29	103.6
Tankah	Sep-19	20.278023	–87.381770	14.60	5.33	0.10	bdl	bdl	17.40	1.69	8.29	1.54	150.51
Tankah	Oct-19	20.278023	–87.381770	10.10	3.75	0.13	bdl	bdl	27.23	1.41	6.25	0.82	211
Tankah	Nov-19	20.278023	–87.381770	7.88	2.22	0.02	bdl	bdl	16.70	1.10	4.76	0.67	300.6
Tankah	Dec-19	20.278023	–87.381770	21.60	6.74	10.74	bdl	bdl	24.55	2.42	12.44	3.02	108.8
Chetumal	Nov-18	18.523783	–88.269428	1.88	2.78	0.67	bdl	bdl	7.74	bdl	2.00	0.57	63
Chetumal	Dec-18	18.523783	–88.269428	8.02	6.04	1.89	bdl	bdl	30.40	3.57	5.12	1.12	55.6
Chetumal	Jan-19	18.523783	–88.269428						15.69	bdl	2.31	bdl	44.6
Chetumal	Feb-19	18.523783	–88.269428	3.05	2.44	1.36	bdl	bdl	10.54	bdl	1.90	0.50	43.7
Chetumal	Mar-19	18.523783	–88.269428	7.37	19.40	9.48	bdl	bdl	4.30	bdl	1.60	0.46	9.9
Chetumal	Apr-19	18.523783	–88.269428	3.51	4.31	3.48	bdl	bdl	11.53	1.29	5.03	1.50	127.8
Chetumal	May-19	18.523783	–88.269428	4.67	4.24	2.10	bdl	bdl	14.79	bdl	2.88	1.00	4.3
Chetumal	Jun-19	18.523783	–88.269428	3.43	2.05	0.15	bdl	bdl	3.85	bdl	2.05	0.44	144.1
Chetumal	Jul-19	18.523783	–88.269428	6.01	4.04	0.32	bdl	bdl	12.47	1.23	4.44	0.85	31.7
Chetumal	Aug-19	18.523783	–88.269428	1.77	1.05	0.08	bdl	bdl	23.40	bdl	1.17	bdl	24.5
Chetumal	Sep-19	18.523783	–88.269428	4.91	6.08	2.47	bdl	bdl	10.35	0.74	3.84	1.58	102.4
Chetumal	Oct-19	18.523783	–88.269428	2.18	1.47	0.04	bdl	bdl	7.40	0.53	1.45	0.62	113.9
Chetumal	Nov-19	18.523783	–88.269428	5.42	1.98	0.31	bdl	bdl	7.83	0.42	1.81	0.44	98.8
Chetumal	Dec-19	18.523783	–88.269428	139.00	116.00	657.00	bdl	bdl					42.6

bdl: bellow detection limit.

Table SII. Isotopes dataset.

Site	Date	Longitude W	Latitude N	d18O (‰)	d2H (‰)	d-excess	pp (mm month^{-1})
Cancún	Nov-18	–86.821001	21.174705	–3.00	–6.82	17.2	49.2
Cancún	Dec-18	–86.821001	21.174705	–1.39	2.85	13.9	58.01
Cancún	Jan-19	–86.821001	21.174705	–1.70	3.75	17.3	100.22
Cancún	Feb-19	–86.821001	21.174705	–2.57	–6.76	13.8	136.8
Cancún	Mar-19	–86.821001	21.174705	–0.82	12.91	19.5	10.3
Cancún	Apr-19	–86.821001	21.174705	–1.20	4.85	14.5	47.5
Cancún	May-19	–86.821001	21.174705	–1.70	–1.11	12.5	30.7
Cancún	Jun-19	–86.821001	21.174705	–2.76	–9.56	12.5	27
Cancún	Jul-19	–86.821001	21.174705	–1.02	3.86	12.1	8.7
Cancún	Aug-19	–86.821001	21.174705	–4.89	–25.74	13.4	11
Cancún	Sep-19	–86.821001	21.174705	–2.74	–9.77	12.1	61.4
Cancún	Oct-19	–86.821001	21.174705	–4.55	–24.17	12.2	239.51
Cancún	Nov-19	–86.821001	21.174705	–3.56	–12.19	16.3	173.41
Cancún	Dec-19	–86.821001	21.174705	–4.78	–23.12	15.1	143.61
Cancún	Jan-20	–86.821001	21.174705	–1.61	4.89	17.8	78.5
Cancún	Feb-20	–86.821001	21.174705	0.14	12.58	11.5	34.6
Cancún	May-20	–86.821001	21.174705	–3.49	–15.66	12.3	122.6
Cancún	Jun-20	–86.821001	21.174705	–5.94	–36.17	11.3	107.6
Cancún	Jul-20	–86.821001	21.174705	–2.39	–7.84	11.3	33.8
Cancún	Aug-20	–86.821001	21.174705	–3.97	–22.15	9.6	66.02
Cancún	Sep-20	–86.821001	21.174705	–2.59	–9.54	11.1	109.62
Cancún	Oct-20	–86.821001	21.174705	–6.49	–38.23	13.7	425.61
Cancún	Nov-20	–86.821001	21.174705	–3.17	–10.28	15.1	213.81
Cancún	Dec-20	–86.821001	21.174705	–3.97	–15.80	15.9	95.44
Cancún	Jan -21	–86.821001	21.174705	–2.32	–4.25	14.3	123.6
Cancún	Jun-21	–86.821001	21.174705	–6.00	–37.87	10.2	163.51
Bacalar	Jan-19	–88.395663	18.666993	–0.98	3.87	11.7	22.1
Bacalar	Feb-19	–88.395663	18.666993	–0.98	3.87	11.7	16.2
Bacalar	Mar-19	–88.395663	18.666993	–1.05	4.46	12.9	16.7
Bacalar	Apr-19	–88.395663	18.666993	–0.45	6.25	9.9	22
Bacalar	May-19	–88.395663	18.666993	–5.46	–38.10	5.5	98
Bacalar	Jun-19	–88.395663	18.666993	–5.34	–32.20	10.5	108
Bacalar	Jul-19	–88.395663	18.666993	–2.50	–10.01	10.0	38.3
Bacalar	Aug-19	–88.395663	18.666993	–4.06	–22.99	9.5	173
Bacalar	sep-19	–88.395663	18.666993	–2.83	–11.73	10.9	86
Bacalar	Oct-19	–88.395663	18.666993	–7.33	–45.28	13.4	139.7
Bacalar	Nov-19	–88.395663	18.666993	–3.18	–11.73	13.7	70.3
Bacalar	Dec-19	–88.395663	18.666993	–2.39	–5.56	13.6	49.1
Bacalar	Jan -20	–88.395663	18.666993	–0.53	8.30	12.6	49.6
Bacalar	Feb-20	–88.395663	18.666993	–2.79	–2.12	20.2	43.5
Bacalar	May-20	–88.395663	18.666993	–4.12	–20.48	12.4	269
Bacalar	Jun-20	–88.395663	18.666993	–8.22	–54.33	11.4	303.4
Bacalar	jul-20	–88.395663	18.666993	–3.82	–18.56	12.0	129
Bacalar	aug-20	–88.395663	18.666993	–2.57	–12.30	8.3	97
Bacalar	Sep-20	–88.395663	18.666993	–2.69	–8.64	12.8	107.6
Bacalar	Oct-20	–88.395663	18.666993	–3.17	–11.18	14.2	177.3
Bacalar	Nov-20	–88.395663	18.666993	–4.86	–22.44	16.4	424.7
Bacalar	Dec-20	–88.395663	18.666993	–1.71	2.73	16.4	74.2
Bacalar	Jan -21	–88.395663	18.666993	–1.87	–3.71	11.2	
Bacalar	Feb-21	–88.395663	18.666993	–1.07	5.86	14.5	

Table SII. Isotopes dataset.

Site	Date	Longitude W	Latitude N	d18O (‰)	d2H (‰)	d-excess	pp (mm month^{-1})
Tankah	Nov-18	–87.381770	20.278023	–0.38	5.51	8.6	76.7
Tankah	Dec-18	–87.381770	20.278023	–1.03	4.58	12.9	127.9
Tankah	Jan -19	–87.381770	20.278023	–1.12	5.96	15.0	159.4
Tankah	Feb-19	–87.381770	20.278023	0.12	9.45	8.5	52.4
Tankah	Apr-19	–87.381770	20.278023	–1.77	–1.53	12.7	99
Tankah	Jun-19	–87.381770	20.278023	–1.96	–3.01	12.7	54.7
Tankah	Jul-19	–87.381770	20.278023	–1.86	–4.48	10.4	22.1
Tankah	Aug-19	–87.381770	20.278023	–2.88	–13.07	10.0	103.6
Tankah	Sep-19	–87.381770	20.278023	–3.14	–11.63	13.5	150.51
Tankah	Oct-19	–87.381770	20.278023	–4.47	–21.43	14.4	211
Tankah	Nov-19	–87.381770	20.278023	–0.68	8.83	14.3	300.6
Tankah	Dec-19	–87.381770	20.278023	–1.06	5.91	14.4	108.8
Tankah	Jan -20	–87.381770	20.278023	–4.14	–14.49	18.6	56.2
Tankah	Feb-20	–87.381770	20.278023	–2.15	6.93	24.1	5.5
Tankah	Apr-20	–87.381770	20.278023	–0.81	5.18	11.6	1.8
Tankah	May-20	–87.381770	20.278023	–4.47	–21.85	14.0	203.5
Tankah	Jun-20	–87.381770	20.278023	–5.13	–30.76	10.3	185
Tankah	Jul-20	–87.381770	20.278023	–1.52	0.77	12.9	95.3
Tankah	Aug-20	–87.381770	20.278023	–1.80	–3.15	11.2	123.3
Tankah	Mar-21	–87.381770	20.278023	–2.06	–4.93	11.6	12
Tankah	Apr-21	–87.381770	20.278023	0.27	20.35	18.2	13
Tankah	May-21	–87.381770	20.278023	–3.14	–17.48	7.6	33.1
Tankah	Jun-21	–87.381770	20.278023	–3.49	–21.25	6.7	271.4
Tankah	Jul-21	–87.381770	20.278023	–2.56	–12.22	8.3	73.5
Tankah	Sep-21	–87.381770	20.278023	–2.23	–4.99	12.9	117.9
Tankah	Oct-21	–87.381770	20.278023	–2.34	–8.12	10.6	110.4
Tankah	Nov-21	–87.381770	20.278023	–2.39	–11.34	7.8	352
Chetumal	Nov-18	–88.269428	18.523783	–1.48	6.51	18.3	63
Chetumal	Dec-18	–88.269428	18.523783	–1.60	2.26	15.0	55.6
Chetumal	Jan -19	–88.269428	18.523783	–1.53	3.38	15.6	44.6
Chetumal	Feb-19	–88.269428	18.523783	–1.53	3.38	15.6	43.7
Chetumal	Mar-19	–88.269428	18.523783	–0.96	8.35	16.0	9.9
Chetumal	Apr-19	–88.269428	18.523783	–0.74	8.46	14.4	127.8
Chetumal	May-19	–88.269428	18.523783	–8.27	–56.26	9.9	4.3
Chetumal	Jun-19	–88.269428	18.523783	–6.88	–45.24	9.8	144.1
Chetumal	Jul-19	–88.269428	18.523783	–2.16	–8.00	9.3	31.7
Chetumal	Aug-19	–88.269428	18.523783	–4.72	–21.07	16.7	24.5
Chetumal	Sep-19	–88.269428	18.523783	–3.44	–12.98	14.5	102.4
Chetumal	Oct-19	–88.269428	18.523783	–4.02	–16.85	15.3	113.9
Chetumal	Nov-19	–88.269428	18.523783	–3.20	–8.38	17.2	98.8
Chetumal	Dec-19	–88.269428	18.523783	–3.01	–9.71	14.4	42.6
Chetumal	Jan -20	–88.269428	18.523783	–0.68	7.51	12.9	52.2
Chetumal	Feb-20	–88.269428	18.523783	–1.48	6.08	17.9	44.3
Chetumal	May-20	–88.269428	18.523783	–2.48	–8.92	10.9	160.3
Chetumal	Jun-20	–88.269428	18.523783	–7.90	–54.37	8.9	376
Chetumal	Jul-20	–88.269428	18.523783	–1.09	1.14	9.9	68.6
Chetumal	Aug-20	–88.269428	18.523783	–1.42	–2.64	8.7	128.8
Chetumal	Oct-20	–88.269428	18.523783	–3.07	–11.69	12.9	162.2
Chetumal	Nov-20	–88.269428	18.523783	–4.59	–25.23	11.5	482
Chetumal	Dec-20	–88.269428	18.523783	–2.97	–5.55	18.2	38.5

Fig. S1. Hysplit trajectory frequencies from December 2018 to November 2019.

December 2018

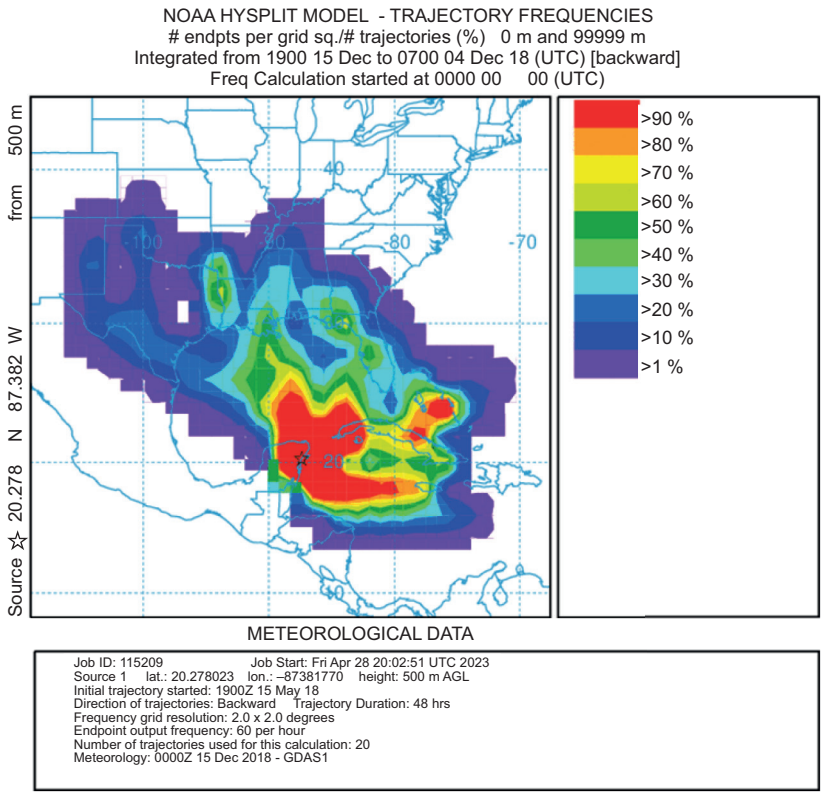

January 2019

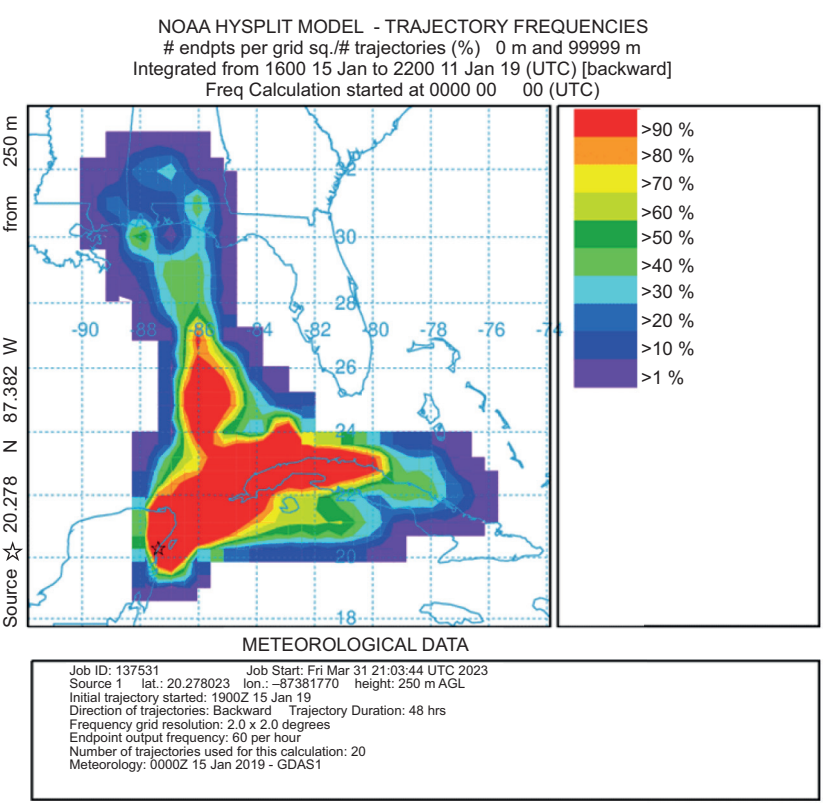

February 2019

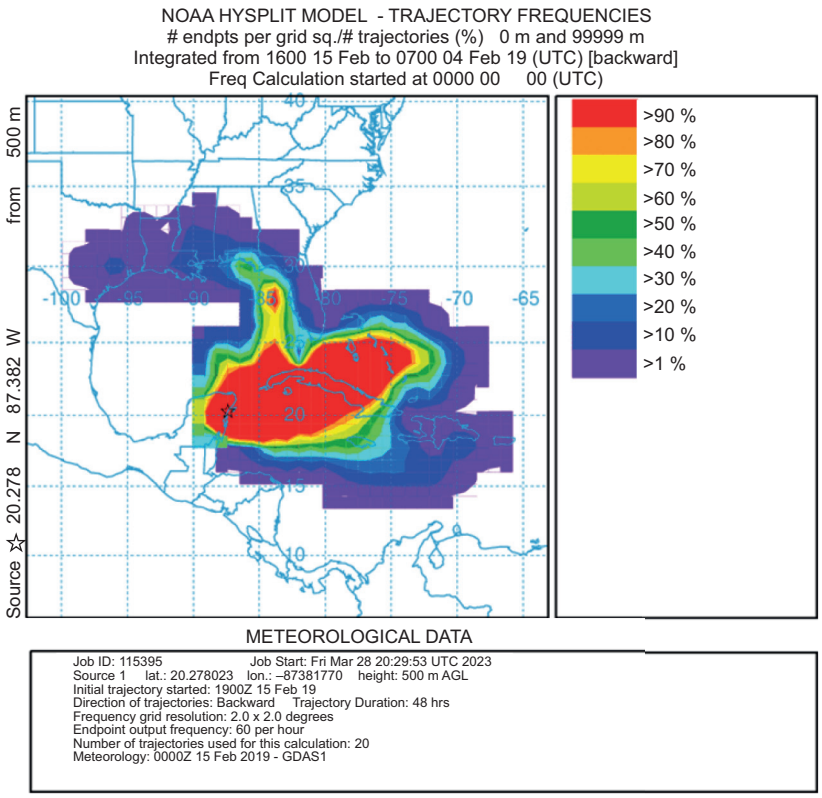

March 2019

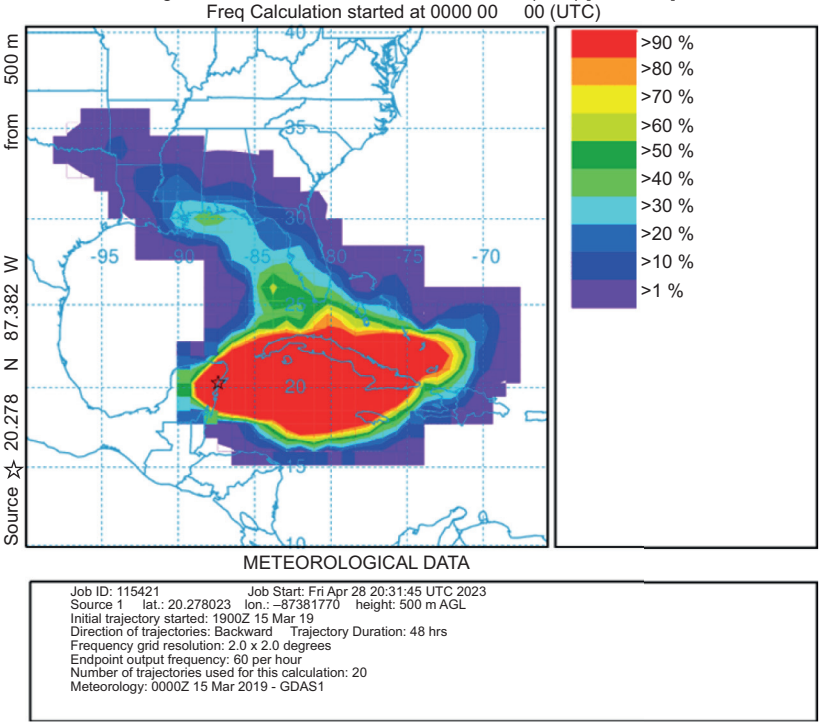

April 2019

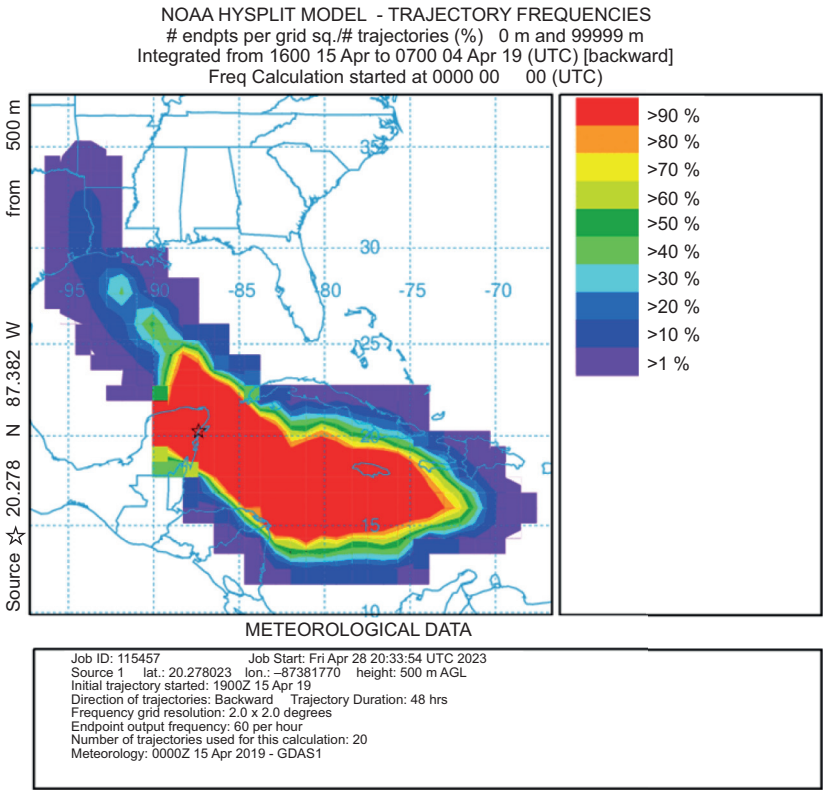

May 2019

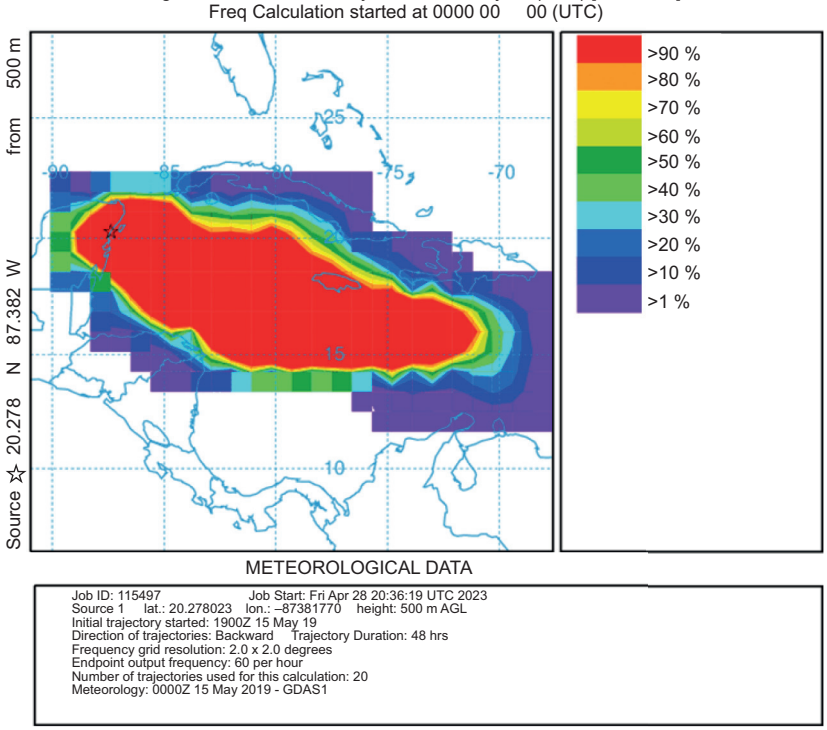

June 2019

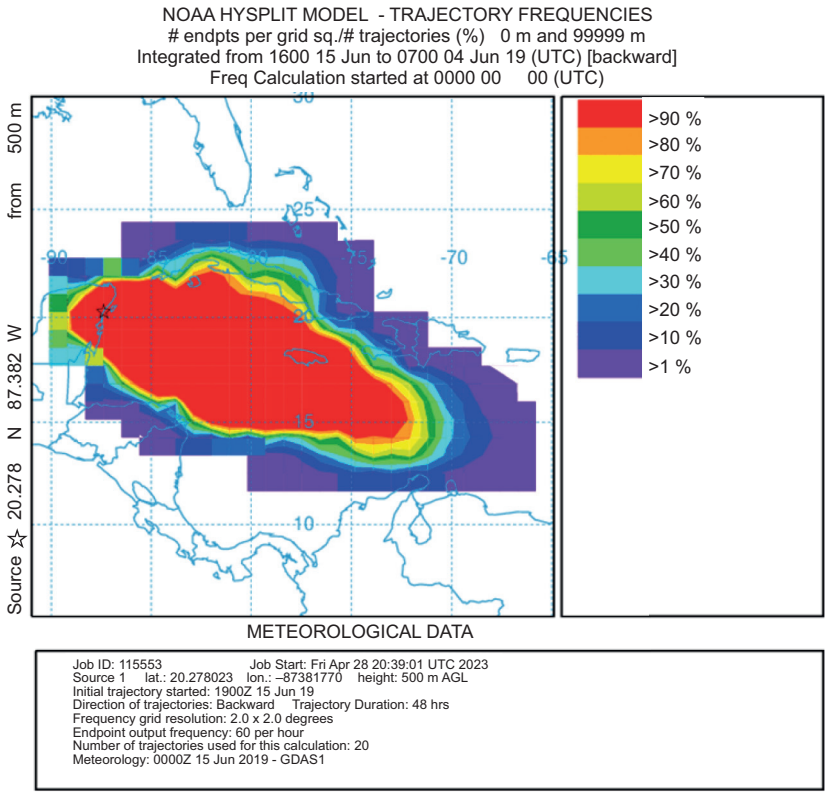

July 2019

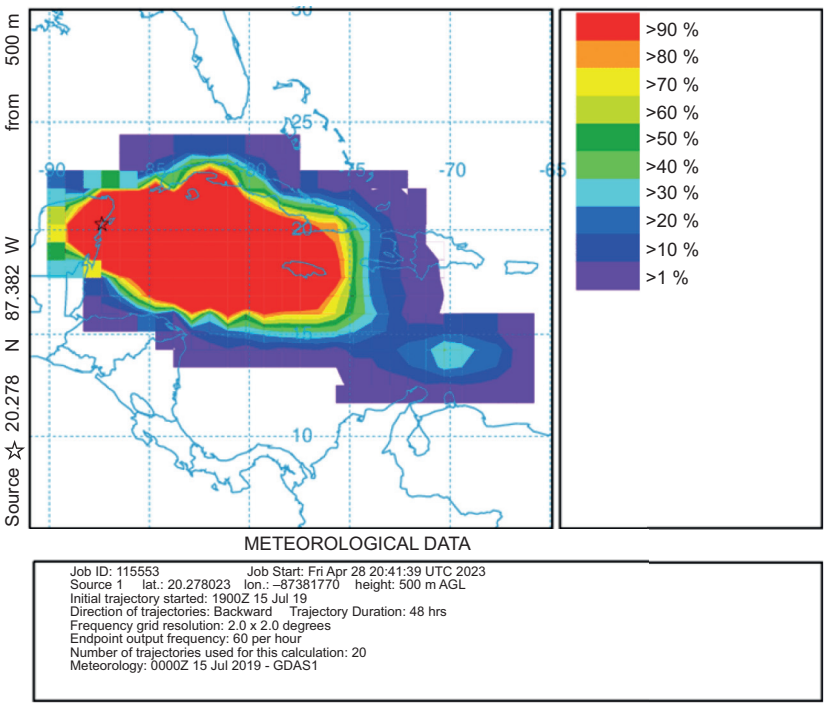

August 2019

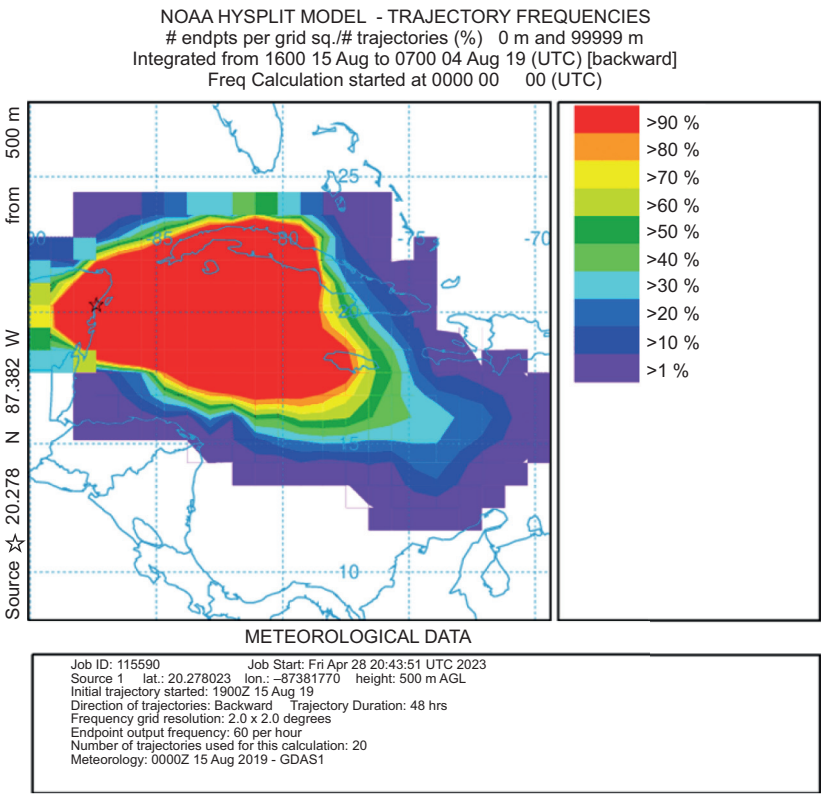

September 2019

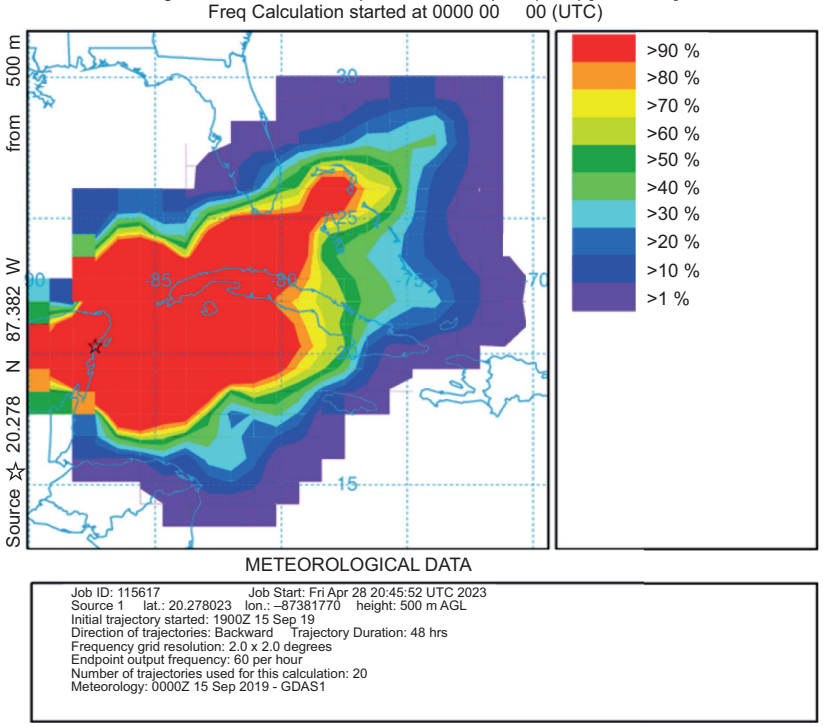

October 2019

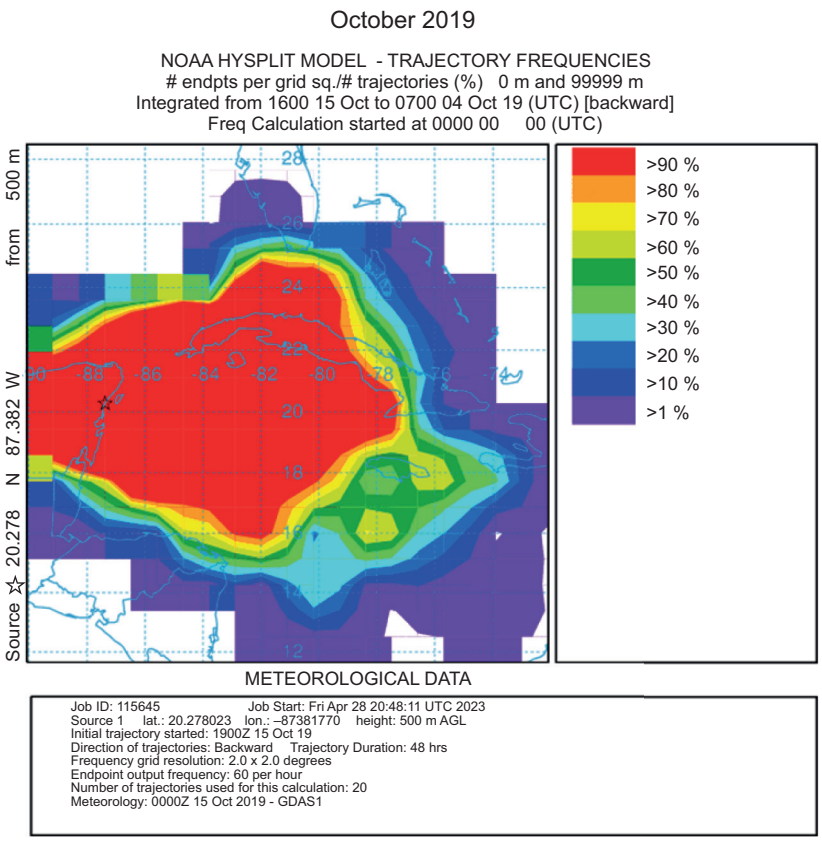

November 2019